Trace metal variability controlled by hydrodynamic processes in a polluted inner shelf environment (Besòs prodelta, NW Mediterranean)

Albert Palanques*, Laura López, Jorge Guillén and Pere Puig

Institute of Marine Sciences (CSIC), Passeig Maritim de la Barceloneta, 37-49, Spain

*Corresponding author. Tel.: +34 932309500; fax: +34 932309555. E-mail address: albertp@icm.csic.es

Abstract

Trace metal pollution of coastal sediment is monitored in many countries to control its evolution and the effectiveness of preventive and corrective measures. However, temporal variability of trace metal pollution is not always due to changes in pollution management, as natural processes can induce a significant variability in the trace metal content of sediment and particulate matter, especially in strongly polluted coastal areas. To study this variability, time series of trace metals in particulate matter and bottom sediments were recorded along with hydrographic and hydrodynamic parameters in the most highly polluted zone of the Besòs River prodelta. Two benthic tripods equipped with current meters, turbidimeters and sediment traps were deployed at 20 and 30 m water depth from late-September to mid-June and sediment cores were taken four times at each site during the deployment period. Trace metal content in the trapped particulate matter and the surface sediment increased during storm events, which can

resuspend and erode several cm of subsurface sediments with higher pollution levels from earlier industrial times. After the storms, significant accumulation of less polluted sediment began, and near-bottom currents redistributed it, decreasing trace metal contents in surface sediments and trapped particulate matter. Therefore, energy conditions previous to monitoring sampling must be considered in order to evaluate the evolution of trace metals in inner shelf polluted sediments.

Keywords: trace metals, pollutants resuspension, seasonal pollution variability, polluted sediment dynamics, inner continental shelf, Mediterranean Sea.

1. Introduction

Contamination of trace metals (TM) in aquatic ecosystems is a global concern because of their abundance, persistence and environmental toxicity (Schwarzenbach et al., 2006; Wang et al., 2015; Chen et al., 2017). They enter from fluvial systems via surface runoff or associated with atmospheric transport into the marine environment (Clark, 2001; Spencer et al., 2003; Maanan, 2008) and even from submarine groundwater (Rodellas et al., 2015). Terrestrial-derived TM from river discharge and surface runoff are mainly deposited within near-shore, shelf and slope environments, whereas TM associated with atmospheric inputs are predominant in open oceans (Viers et al., 2009).

Most TM transported downstream in a river are bound to fine suspended particulates and colloids because they are relatively insoluble in water/surface sediments with oxic conditions of circa neutral pH (Poulton and Raiswell, 2000;

Tansel and Rafiuddin 2016; Masson et al., 2018). Once the sediment load has been discharged into the marine environment, oceanographic processes can transport and redistribute it along with the associated pollutants. After sedimentation, pollutants can be resuspended by physical erosion (waves and currents) or bioturbation, and also by anthropogenic activities such as dredging and trawling (Eggleton and Thomas, 2004). The remobilization of previously deposited pollutants can cause an environmental issue because, even when the source of pollution has been removed, pollutants stored in the sediment can be released into the water column by erosion and due to changes in the redox environmental conditions (Bancon-Montigny et al., 2019).

Large river systems discharging into energetic oceans can disperse fine particles and TM over large areas, thus diluting the anthropogenic TM load. However, in the Mediterranean Sea, the micro-tidal regime and the moderate wave energy allow the fine particles polluted by anthropogenic TM to accumulate in shallow environments before being sufficiently diluted, generating anomalous contents on the seabed (Frignani et al., 1997; Palanques et al., 1998, Bay et al., 2003; García-Orellana et al., 2011; Oursel et al., 2014).

For this reason, the trace metal anomalies in the sediments of the Mediterranean Sea are near to contaminant discharge sources, usually around river mouths (Palanques et al., 1990; Puig et al., 1999; Roussiez et al., 2006; Radakovitch et al., 2008; Lopes Rocha et al., 2017) and especially near urban and industrial areas (Palanques and Díaz, 1994; Palanques et al., 2017).

The Mediterranean climate induces long periods of low river flow alternating with flash floods (Oursel et al., 2014). The irregular and episodic character of the river discharges makes the pollutants reach the sea in sporadic

pulses that induce variability in the suspended sediment and TM inputs. In addition, TM in sediments of the inner shelf are more frequently exposed to resuspension events generated by storms than those accumulated in deeper environments. The magnitude of the resuspended sediment fluxes and pollutants depends on the wave energy and current speed but also on sediment availability, sediment characteristics, pollutant type and water depth (Nittrouer and Wright, 1994; Harris and Wiberg, 2002; Eggleton and Thomas, 2004). Consequently, temporal variations of TM pollution in bottom sediment are expected in coastal environments (Khaled-Khodja et al., 2018; Najamuddin et al., 2016).

One area heavily affected by TM pollution in the Mediterranean Sea is the Barcelona inner continental shelf, and more precisely the Besòs River prodelta (Fig.1). Anthropogenic trace metal levels in this area are high enough to have adverse biological effects and be considered as pollution (Palanques et al., 2017). Trace metal pollution in sediments and suspended particles in this area has been widely studied in the past (Cros and García-Rey, 1980; Modamio, 1986a; Palanques and Díaz, 1994; Palanques, 1994; Palanques et al. 2016; Palanques et al. 2017). However, the variability of TM and their relationships with hydrodynamic events have not been previously addressed. Therefore, the objective of this paper is to study TM variability in settling particulate matter and bottom sediment linked to hydrodynamic activity in the most highly polluted zone of the Besòs prodelta in order to improve the understanding of TM pollution dynamics in shallow marine environments.

2. Methods

2.1. Study area

The study area is located on the Barcelona inner continental shelf in the prodelta of the Besòs River (Fig. 1). In this area, with a tidal range lower than 0.2 m, wave conditions show mean significant wave heights (Hs) of 0.7 m, a mean period of 4.3 s and a maximum wave height of 4.6 m (Gómez et al., 2005). Storms occur mainly from October to April, and the strongest ones come from the E. The most persistent current direction is along-shelf toward the SW, with an average velocity of between 5 and 10 cm s^{-1} (Grifoll et al., 2013).

The study area receives discharges mainly from the Besòs River, which traverses urban, industrial and rural settings in a watershed of 1029 km^2. Mean water discharge between 1968 and 2008 was 6.8 m^3 s^{-1}, with a maximum water discharge of 270 m^3 s^{-1}, a mean sediment flux of 474.7 g s^{-1} and a mean annual sediment discharge of 15000 t yr^{-1} (Liquete et al., 2007, 2009). The sediments discharged by the Besòs River form a muddy prodelta that extends south-westward from the river mouth between 20 and 60 m depth along the inner and mid-continental shelf (Palanques and Díaz, 1994). Wave-induced bottom shear stress is the main stirring factor for sediment resuspension and is mainly effective in the inner shelf region (Grifoll et al., 2014; López, 2017).

The sediments of the proximal parts of the Besòs prodelta have been highly polluted by Hg, Cr, Pb and Zn from industrial and urban activities since industrial times in the early twentieth century (Palanques et al, 1998). Since the 1980s, this strong contamination has been attenuated by the implementation of corrective actions in industries and urban areas, including the construction of 24 wastewater treatment plants in the Besòs watershed (Palanques et al. 2017). The

biggest of them, installed at the river mouth, has a capacity to treat up to 525.000 m^3 d^{-1} (6 m^3 s^{-1}) of water, trapping and removing a large part of the polluted particulate matter from the Barcelona sewage system before discharging into the sea. However, present-day TM levels are still relatively high because of the difficulty of managing all the water and sediment pollution in this highly populated and industrialized area, especially during heavy rain events.

2.2 Field work and instrumentation

Two benthic tripods were deployed at 20 and 30 m water depth (Fig. 1) which are the depths of the Besòs inner prodelta where sediment TM pollution reach the highest levels (Palanques et al., 1998; 2017). These tripods were deployed on 27 September, retrieved and redeployed on 28 November and 28 February and finally retrieved on 19 June. Therefore, the total sampling period consisted of three consecutive deployments that spanned from 28 September 2007 to 19 June 2008. Each tripod was equipped with an Aanderaa Doppler current meter (RCM-9) coupled with an optical backscatter turbidimeter placed at 0.53 m above bottom (mab) and a sediment trap 97 cm high and 13 cm wide (aspect ratio 7.5) with 12 rotary collectors. The current meter sampling interval was 30 minutes and the trap sampling interval was set at 5 days for the first deployment and 7.5 days for the second and third deployments. During the first and second deployments, the instruments of the tripods recorded data all the time, but during the third deployment, only the instruments of the tripod located at the 20 m isobaths worked properly.

In addition, sediment cores were obtained at the tripod sites coinciding with the tripods deployment and retrieval operations on 27 September, 28 November, 28 February and 19 June to study the changes of bottom sediment during the deployment period. Sediment cores were collected with a HAPS corer. They were sliced in 1-cm-thick intervals aboard the vessel. Core subsamples were stored at 4 degrees Celsius for further laboratory analysis (see Section 2.2). The core sampled in September was analysed from 0 to 20 cm, whereas the other cores were only analysed from 0 to 12 cm to see changes in near-surface sediments.

Wave measurements were obtained from the Llobregat directional buoy located 16.5 km SSW from the study area at 45 m water depth (41º16.69'N; 2º08.48'E), which recorded data every hour (López et al., 2017). Interruptions in the buoy time series were filled in with data from the WANA model, which provides directional wave information every three hours (Spanish Port Authority, 2016). Wave height and period from the WANA model were calibrated through linear regression using the buoy observations from October 2001 to December 2008 (Sancho-García et al., 2013). The daily discharge of the Besòs River was obtained from the Catalan Water Agency gauging station located 2.8 km upstream from the Besòs River mouth.

2.3 Laboratory work

2.3.1 Preparation and treatment of samples

To prevent sample degradation, the sediment trap cups were filled with a borax-buffered 5% formaldehyde solution in 0.20-µm filtered sea water before being deployed. After the trap recovery, pH was measured in each cup to check

that there was no acidification. The samples were treated following the procedures described by Heussner et al. (1990). The trapped material was split with a peristaltic dispenser to divide the total sample into several homogeneous aliquots. Swimmers (organisms deemed to have actively entered the trap) were removed from the samples by wet-sieving the sample through a 1 mm nylon mesh. Samples were left to settle again (for one to two days) and examined under a magnifying glass to remove organisms smaller than 1 mm. Subsamples for total mass flux (TMF), carbon and mercury were filtered onto Whatman GF/F glass microfibre filters, while those for major and trace heavy metal analysis were filtered onto HAWP Millipore nitro-cellulose white NF filters. The filters were dried to constant weight at 40º Celsius and then placed for 24 h in a desiccation bowl. TMF was computed using the total mass weight divided by the trap collecting area (0.125 m^2) and the sampling interval (in days). As the sediment trap was probably affected by bias during high waves and current events, the reported trapped fluxes should be considered semi-quantitative values.

Bottom sediment samples were dried on a stove at 40º Celsius and ground and homogenized in an agate mortar for major, minor and trace element analysis.

2.3.2 Grain size analysis

The grain size of the sediment samples was determined by a settling tube for the >50 μm fraction and by a Sedigraph 5100D (Micromeritics) for the <50 μm fraction, following the method described by Giró and Maldonado (1985). Data from the two analyses were integrated by the program INTEGRA'03 to produce the full grain size distribution. Grain size of sediment trap samples was determined by a Horiba LA 950 V2 laser particle size analyser.

2.3.3 Organic carbon

To determine total carbon (TC) and organic carbon (OC) concentration, six subsamples were filtered onto pre-weighed and pre-combusted (overnight at 550ºC) Whatman GF/F glass microfibre filters (47 mm diameter). Two subsamples were used to determine TC in a LECO CN 2000 analyser. Inorganic carbon (IC) was obtained by acid digestion (HCl 6M) of another two subsamples in a LECO CC-100 connected to the CN analyser. The difference between TC and IC was considered total organic carbon (TOC). Uncertainties were lower than 0.1%

2.3.4 Aluminium and trace elements

For the analysis of aluminium (Al) and TM in trapped particulate matter and bottom sediment, a total digestion technique was carried out according to Querol et al. (1996), using HNO3, HF and HCl suprapure acids, digesting 0.1 g of sediment sample in a closed system and heating at 90ºC. For every 18 samples, a blank, a PACS-2 reference material (National Research Council, Canada) and a random-replicated sample were used for analytical quality control. Trace elements (except Hg) were analysed by ICP-MS. Al was analysed by ICP-AES. The overall analytical uncertainty was below 15% and typically between 5% and 10%.

For Hg analysis, a LECO AMA254 Mercury Analyser complying with US EPA Method 7473 (US EPA, 2007) was used. PACS-2 reference material from the National Research Council Canada, random-replicated for every 10 samples,

and blank samples to avoid memory effects were used for analytical quality control. The overall analytical uncertainty was below 10%.

To remove the influence of grain size on the TM analysis, the samples were normalized using the relation

$TM_n = (TM \times 100) / Mud,$

where mud is the silt + clay grain size fraction and TM_n is the normalized concentration, approximately representing the concentration of a sample if it were 100% fine sediment. We thus show both TM content in the bulk sample and TM_n to analyse the variability in both ways.

Background trace metal levels of prodeltaic sediments had been previously determined from uncontaminated samples of the bottom of sediment cores (Palanques et al., 2008, 2016, 2017) and were used here to estimate the enrichment factors (EFs). Aluminium-trace metal regression curves were established for every trace element in order to identify the background levels normalized to aluminium content (Al normalization) (Table S1 of Supplementary data). The ratio between metal concentration and background level (Al normalized) for each sample was defined as the EF.

2.3.5. Calibration of Aanderaa turbidity sensors

Aanderaa turbidity sensors express the light scattering intensity as the equivalent of nephelometric or formazin turbidity units (NTU or FTU). This calibration was conducted by the manufacturer (Aanderaa) using formazin (turbidity calibration standards). In order to convert FTU units into concentration

units (mg L^{-1}), the turbidity sensors were transformed using the measurements carried out by Guillén et al. (2000) in a nearby area. The intensity of the light backscattered by particles was calibrated with a nephelometric solution to calculate suspended sediment concentration (SSC) with the equation

SSC (mg L^{-1}) = 1.21 x NTU + 0.43 (r^2 = 0.46).

2.3.6 Total maximum shear stress

A one-dimensional (1D) sediment transport model (Wiberg and Smith, 1983; Wiberg et al., 1994; Harris and Wiberg, 1997, 2002;) was used to estimate the total maximum shear stress. The model represents the frictional momentum balance in the bottom boundary layer using an eddy viscosity profile enhanced by wave-current interaction. Then, the total shear stress was computed in such a way as to account for differences in direction between the waves and the current. In the study area, wave-induced shear velocities (U_{*w}) were generally two times greater than current-induced shear velocities (U_{*c}) at 20 m water depth, so waves made a greater contribution to total shear stress (see López et al., 2017 for further details).

3. Results

3.1 River discharge, waves, currents and shear stress

The Besòs River water discharge showed an episodic pattern, with increases occurring mainly in autumn and spring (Fig. 2a). Average river water

discharge during the study period was 3.8 m^3 s^{-1}, with discharge peaks of up to 16 and 18 m^3 s^{-1} in October and May, respectively. The increases in river water discharge were accompanied by increases in wave activity except in early October and early June.

During the study period, 12 wave storm events increased SSC significantly and 9 of them occurred during the autumn months (Table 1). In winter, conditions were relatively calm, with less resuspension by wave storms, whereas in spring months two storms increased SSC significantly.

The most energetic episode occurred from 15 to 18 December 2007, with a maximum wave height of 3.38 m and a period of about 11 s, followed by a smaller storm (wave height 2.5 m and period >8 s) after less than 2 two days of relatively calm conditions. Both storm episodes had an eastern component in the direction of wave propagation (Fig. 2b and c).

The time series of current speed at the 20 and 30 m sites averaged 7.1 and 5.6 cm s^{-1}, respectively, with peaks mainly associated with wave storm events. The maximum current peaks at the two study sites were similar: 27.9 cm s^{-1} and 28.1 cm s^{-1} at the 20 and 30 m sites, respectively (Fig 2d). Current speed reached several peak values during the autumn, decreased in winter and maintained lower values in spring.

Time series of total shear stress at 20 m depth showed several peaks, which were mainly associated with wave storms. The highest frequency and intensity of bottom shear stress peaks was in autumn. The maximum bed shear stress was 2.13 N m^{-2} during the mid-December storm event. The intensity of the shear stress peaks decreased significantly in winter and spring, increasing only during the mid-May event (Fig. 2e; Table 1).

3.2. Near-bottom suspended sediment

Near-bottom SSC increased during storm events, generating peaks mainly in autumn and mid-spring. At the 20 m site, SSC of up to 80 mg L^{-1} and 100 mg L^{-1} were recorded on 25–26 October and 9–10 May, respectively. Some storms gave higher SSC at 30 m than at 20 m depth. López et al. (2017), concluded that this occurred mainly during dry storms, when fresh sediment had been winnowed from shallow areas (20 m water depth) and deposited offshore (30 m water depth), where sediment availability increased. This was the case of the 15–18 December event (80 and 50 mg L^{-1} at 30 and 20 m depth, respectively) and the 3–5 January event (40 and 20 mg L^{-1} at 30 and 20 m depth, respectively). Without storm periods, SSC ranged mainly between 1 and 5 mg L^{-1} (Fig. 2f). SSC also increased at the end of the deployment as a consequence of a river discharge increase without wave storm.

3.3. Trapped particulate matter fluxes

Trapped particulate matter fluxes showed increases from October to December and in May (Fig. 2g). These increases were coincident in time at the two study sites, although they were higher at 20 m depth. The maximum TMF at 20 m depth (1100 g m^{-2} d^{-1}) occurred at the end of October after the 25 October storm event. At 30 m depth, the highest values (550 g m^{-2} d^{-1}) were obtained during the mid-December and early January storm events.

TMF decreased after these events and the minimum fluxes were in early May (35 g m^{-2} d^{-1}). Finally, TMF increased in mid- and late May, coinciding with storm and water discharge events, but reached lower values than in autumn (430 g m^{-2} d^{-1} at 20 m depth).

3.4. Grain size, TOC and Al of trapped particulate matter

The sediment trap samples allow to know the composition of the particulate matter that was moving in the water column due to the hydrodynamic processes and settled in the trap during the sampling intervals.

The mud content of the trapped particulate matter showed a decreasing trend, from more than 80% in early October to 30% in mid-December (Fig. 3a), coinciding with the more energetic period in terms of storm activity and reaching the lower mud content during the strongest storm event. After this event, the mud content increased and maintained values of between 60% and 80% from mid-January to May.

The OC content showed a similar trend to grain size, tending to decrease from October to mid-December (from 3.2% to 1.4%) and to increase from January to May (from 1.4% to 5.2%). The maximum values were in April, probably because of a spring bloom, and the minimum values in mid-December (Fig. 3b), coinciding with the strongest storm and the coarser trapped particulate matter. The Al content was quite constant, ranging from 6% to 7.5% (Fig. 3c) during the deployment period.

3.5 Trace metal concentration in the trapped particulate matter

Time series of TM and TM_n concentrations in the trapped particulate matter showed similar trends at the 20 and 30 m sites. There was an increasing trend, with several fluctuations from October to mid-December, a decreasing trend in January, relatively constant lower concentrations from February to April and a few increasing peaks in April and May (Figs. 4 and 5). In the TM temporal series, Cr and Hg concentrations were slightly higher at 30 than at 20 m depth and Cd was often lower at 30 m depth, whereas the other TM concentrations were more similar at both sites (Fig. 4). However, all the TM_n concentrations tended to be slightly lower at 30 than at 20 m depth (Fig. 5). Most of the increasing peaks of TM and TM_n occurred during events of increasing waves, with or without river discharge increases. During events of river discharge increases without increasing waves (October 17, 15.8 m^3 s^{-1}; June 6, 17.3 m^3 s^{-1}), TM and TM_n decreased. In the TM temporal series, the highest Hg, Cu and Zn levels in autumn were reached in early November during a period of high river discharge and wave storm events and the highest Cd, Pb and Cr values were observed in mid-December, during the strongest storm event without river discharge increases (Fig. 4). However, all the TM_n reached their highest levels during the mid-December storm event (Fig. 5). TM and TM_n also peaked during the mid-May wave storm, coinciding with river discharge increases, but most of these peaks were lower than that of the December one. The lowest TM and TM_n levels were observed mainly in February and March, with lower storm and river discharge activity. The increasing trend of the pollutant levels in the trapped particulate matter during storm events is also shown by the correlations between TM_n and

the mean and maximum shear stresses during each sediment trap sampling period (Table 2)

TM fluxes showed the same trends as TMF, with maximum values between 26 October and the 1 November at 20 m depth except for Cd and Cu, whose maximum fluxes were in mid-December. At 30 m depth, TM fluxes were lower than at 20 m depth, and the maximum TM fluxes were observed in the mid-December event for all TM (Fig. 6).

3.6. Grain size, TOC and Al of sediment cores

The mud content of the sediment core taken at 20 m depth in September showed values of between 30% and 40% in the upper samples and an inflexion point, from which there was a downward increasing trend to values of between 60% and 80% in the lower samples. TOC of this core showed a similar distribution, with values of between 1.0% and 1.3% in the upper samples, increasing to 2.5% in the lower samples. The vertical distribution of mud and TOC of this core showed a peak at 12 cm depth. The vertical distribution of the mud and TOC contents of the sediment cores taken at 20 m in November, February and June showed similar values but with inflexion points and peaks at different depths (Fig. 7).

In the sediment cores taken at 30 m depth, the mud content showed a downward increasing trend from about 60% at the surface to about 90% at 10 cm depth. The TOC content ranged from 1.8% to 2.5% in the upper 10 cm of sediment. The samples of the September core taken below 10 cm depth showed a decrease in the mud and TOC contents to 70% and 1.2%, respectively (Fig. 7).

The Al content of all the cores taken at 20 and 30 m depth was quite constant, ranging between 5% and 6% (Fig. 7).

3.7 Trace metals in sediment cores

Vertical TM and TM_n distribution in sediment cores showed a downward increasing trend, reaching a peak of maximum values and a downward decreasing trend at the bottom (Figs. 8 and 9). Each of the four cores taken at the study sites during the study period showed inflexion points from which values increased more sharply, reaching similar maximum concentration peaks at different depths. At 20 m depth the TM peak was at 16 cm depth in September, 8 cm depth in November, 10 cm depth in February and not recorded in June. At 30 m depth it was at 8 cm depth in September, 5 cm depth in November, 5 cm depth in February and 6 cm depth in June (Figs. 8 and 9).

Maximum TM_t and TM_n levels ranged from a few times to several orders of magnitude higher than natural levels (Table S1) and corresponded to a highly polluted sediment layer, with Hg, Zn, Cr and Pb concentrations exceeding the ERM values defined by Long et al (1995), over which the incidence of environmental effects is usually >75% . TM concentrations of the sediment samples upon this layer were up to one order of magnitude lower (Figs. 8 and 9) but still high, all between the ERL and ERM values defined by Long et al (1995) with an incidence of biological effects usually between 25 and 75%, except Hg, which was still over the ERM value. In general, TM all followed similar patterns, indicating a common source. The TM concentrations of the sediment cores were found to be correlated with the mud fraction (Table S2). However, normalized

against the relatively constant Al content in these cores, the TM increases identify major enrichments accounted for by anthropogenic pollution (Table S3). In addition, the similar TM and TM_n variability indicates that the levels are mainly controlled by pollution rather than by grain size.

The variability of TM and TM_n in the sediment cores also includes the pollution levels of surface sediment. Surface TM and TM_n increased from September to November and decreased from November to February. From February to June, TM decreased at 20 m depth and increased at 30 m depth, and surface TM_n increased at 20 m depth but showed no clear trend at 30 m depth (Table 3).

4. Discussion

4.1. Effects of storms on sediments and TM content

The effects of storms and floods on sediment erosion and accumulation in shallow environments have been studied by various methods in different areas (Allison et al., 2000; Wheatcroft and Borgeld, 2000; Guillén et al., 2006; Stevens et al., 2007; Palinkas and Nittrouer, 2007). This is a complex task that involve combining various processes and taking into account the spatial and vertical variability of sediment properties.

In the Besòs inner prodelta, riverine inputs generate ephemeral bottom sediment layers that are eroded during storms and transported away. After the storms, sediment accumulation begins and the near-bottom currents redistribute recently deposited sediment.

The effects of this dynamics are recorded in the trapped particulate matter and in the sediment cores whose highly polluted sediment layer is a marker bed. This layer corresponds to polluted sediment discharged by the Besòs River before the construction of the wastewater treatment plants and the implementation of environmental regulations in the Besòs River watershed (Palanques et al., 2017). The TM and TM_n concentrations of the overlying sediment have decreased by up to one order of magnitude and the mud and TOC contents of this sediment have also decreased by half (Figs 7, 8 and 9), probably due to the mud and TOC removed by the wastewater treatment plants and other regulations.

Consequently, the inflexion points and peaks of the TM and TM_n vertical distribution in the sediment cores (Figs. 8 and 9) can be used as a guide level to make a rough estimation of the resulting sediment erosion or accumulation induced by hydrodynamic events at the study sites during the field work period.

In late summer and in early October, previously to the field work period, increases in river discharge with little wave storm activity left ephemeral surface sediment deposits sampled in the September core. The formation of these deposits previous to the autumn storm passages could enhance the bottom sediment erodibility because of the higher porosity and water content of the fresh sediment (Guillén et al., 2006; Grifoll et al., 2014). As a result, the storms occurring from late October to mid-December, generated high SPM resuspension peaks simultaneous to shear stress increases, indicating recurrent bottom sediment resuspension (Fig. 2). The different depths of the TM and TM_n inflexion points and peaks in the cores taken at 20 and 30 m depth in September and November suggest that the storm events occurring during this

time eroded 8 cm of sediment at 20 m depth and 3 cm at 30 m depth (Figs. 8, 9 and 10). This erosion reached subsurface sediment with higher concentrations than those of the surface sediment in September (Figs. 8 and 9) and resuspended it, leaving exposed more polluted sediment at the surface in November (Table 3). The increasing trend of the TM and TM_n content in the trapped particulate matter between October and November (Figs. 4 and 5) also indicates that sediment traps collected resuspended sediment with progressively higher TM concentrations, according to an increasing erosion of deeper and more polluted sediment.

The mid-December storm generated the highest shear stress (Fig. 2) and the strongest TM peak in the trapped particulate matter (Figs. 4 and 5), suggesting an increasing erosion of deeper and more polluted sediment. Comparing the maximum TM and TM_n levels reached by the particulate matter trapped in mid-December (Figs. 4 and 5) with the TM and TM_n distribution of the sediment cores taken in September (Fig. 8 and 9), we observed that levels matched at about 16 cm depth of the core taken at 20 m depth and 4 cm depth of the core taken at 30 m depth. Therefore, we hypothesize that sediment erosion caused by all the autumn storms between September and mid-December could have reached up to 16 cm at 20 m depth and 4 cm at 30 m depth.

However, the cores taken in February indicated a net accumulation of 2 cm of sediment at 20 m depth and no accumulation at 30 m depth in comparison with the November core (Figs. 8, 9 and 10). This could be explained because shear stresses in January and February were low (<0.5 N m^{-2}), and currents exceeded 14 cm s^{-1} several times, reaching up to 24 cm s^{-1}, so

they probably redistributed bottom sediment and particulate matter, refilling part of the sediment eroded by the previous storms. The decreasing trend of the TM and TM_n concentrations in the particulate matter trapped in January and February (Figs. 4 and 5) and the lower TM and TM_n concentrations of the surface sediment in February (Table 3) suggests that the more polluted resuspended particles were winnowed away from the study area and progressively diluted with less polluted material (probably from the river, whose low water discharge was treated in the wastewater treatment plants, and from less polluted coastal areas transported by the along-shelf currents).

The sediment cores taken in mid-June indicate a possible accumulation of 6 cm of sediment at 20 m depth and 1 cm at 30 m depth in comparison with the core taken in late February. From late February to mid-June the only significant resuspension event was the mid-May storm that increased the total shear stress simultaneously to the SSC and TMF (Fig. 2). During this event, TM and TM_n content of the trapped particulate matter also increased (Figs. 4 and 5) suggesting short erosion and resuspension of more polluted subsurface sediment. However, consecutive floods and the absence of significant wave storms from this event to mid-June (Fig. 2) probably favoured the accumulation of ephemeral sediment layers again near the river mouth and the decrease in the TM and TM_n contents in the particulate matter trapped at 20 m depth at the end of the deployment period.

The thickness of the eroded sediment at 20 and 30 m depth is consistent with the concentration profiles of excess ^{210}Pb in the sediment cores taken in September, which show an intense mixing in the 20 m core and a 3-cm-thick surface mixed layer in the 30 m core (Palanques et al., 2017). The variability in

the TM levels of the trapped and bottom sediment are represented in Figure 10, which shows the case of Hg_n as representative of the TM behaviour at the study sites.

4.2. Implications of the variability of trace metal contents

TM and TM_n variability in the sediment and trapped particulate matter of the study area is mainly controlled by the resuspension of historically more polluted sediment during storms and the redistribution of less polluted ephemeral sediment layers after storms and floods through the action of near-bottom currents. These dynamics can also occur on inner continental shelves of big coastal cities of the Mediterranean Sea and other parts of the world where rivers have reduced their pollution discharge into coastal areas affected by moderate-energy events.

Nevertheless, there are few studies on temporal TM variability in polluted bottom sediments caused by the action of hydrodynamic processes. Some of them found no significant differences during the year related to rainfall events (Tan et al, 2016) or hurricanes (Warren et al., 2012), but pollution levels in these studies were lower than in our study area, so variability could be more difficult to detect. Other studies observed higher TM concentrations during the wet seasons than during the dry season (Najamuddin et al., 2016), or that sediment resuspension caused significant enrichments in TM in the water column (Bancon-Montigny et al., 2019), in agreement with our observations. Li et al (2018) also observed that the TM content was higher in winter than in summer and was higher in the post-typhoon period than in the pre-typhoon

period. Consequently, George et al. (2007) stated that seafloor metal distribution should be related to energy levels and Bancon-Montigny et al. (2019) that the seasonal variations in sediment composition are rarely taken into account in ecotoxicology studies.

One important implication of the results of this study is that the TM variability induced by high-energy events in historically polluted areas must be taken into account for long-term TM monitoring in environmental management programs. TM variability in these areas is not only a function of the pollution inputs from the continent but also of the ancient pollution stored in subsurface sediment, which can be exposed during the more energetic events and become a source of metals that are redistributed by waves and currents, changing the TM content of surface sediments. Pollution levels will be different if the sediment sampling is done after a stormy period than if it is done after a calm sea period.

5. Conclusions

A highly polluted sediment layer was accumulated on the Besòs inner shelf from the 1940s to the 1980s. The implementation of environmental regulations and actions in the Besòs watershed reduced the TM pollution levels of the sediment that lay upon this sediment layer by one order of magnitude.

However, wave storm events recorded in this study eroded several centimetres of sediment, reaching and resuspending sediment from the upper part of this highly polluted layer and thus increasing the TM pollution levels of surface sediment and the trapped particulate matter.

After these storms, less polluted particulate matter settled, forming ephemeral sediment layers that were redistributed by near-bottom currents, replacing previous eroded sediment and decreasing TM pollution contents in surface sediments and trapped particulate matter.

As a result, TM pollution content of surface sediment increased in autumn due to the higher storm activity, decreased in winter due to calmer conditions and maintained relatively similar values in spring. TM and TM_n contents in trapped particulate matter showed similar trends and recorded the peak pollution levels generated by the stronger storms in mid-October, mid-December and mid-May.

Therefore, TM levels of highly polluted shallow areas where preventive and corrective actions have been undertaken can change significantly in function of the seasonal variability and energy of the hydrodynamic processes. TM pollution in these areas should be related to the energy of hydrodynamic processes before sediment sampling. This factor should be taken into account for TM pollution monitoring of inner shelf sediments in environmental management programs, as variability of TM pollution can stem not only from present continental inputs but also from historical pollution stored in the sediment column and resuspended during storm events.

Acknowledgements

This work was supported by the Ministerio de Educación y Ciencia of the Spanish Government within the SEDMET project (CTM2006-06919). We also thank the officers and crew of the R/V *García del Cid* (CSIC) and the R/V

Sarmiento de Gamboa (MINECO) and the staff of the Institut de Ciències del Mar (CSIC) and the Unitat de Tecnologia Marina (CSIC) for their help and dedication during the cruises and in the laboratory work. A.P., J.G and P.P. belong to CRG on Littoral and Oceanic Processes, supported by Grant 2017 SGR 863 of the Generalitat de Catalunya.

References

Allison, M.A., Kineke, G.C., Gordon, E.S., Goñi, M.A., 2000. Development and reworking of a seasonal flood deposit on the inner continental shelf off the Atchafalaya River. Cont. Shelf Res. 20, 2267–2294.

Bancon-Montigny, Ch., Gonzalez, C., Delpoux, S., Avenzac, M., Spinelli, S., Mhadhbi, T., Mejri, K., Hlaili, A. S. Pringault, O., 2019. Seasonal changes of chemical contamination in coastal waters during sediment resuspension. Chemosphere 235, 651-661.

Bay, S.M., Zeng, E.Y., Lorenson, T.D., Tran, K., Alexander, C., 2003. Temporal and spatial distributions of contaminants in sediments of Santa Monica Bay, California. Mar. Environ. Res. 56, 255–276.

Chen, Z., Chen, L., Chen, Ch., Huang, Q., Wu, L., Zhang, W., 2017. Organotin Contamination in Sediments and Aquatic Organisms from the Yangtze Estuary and Adjacent Marine Environments. Environ. Eng. Sci. 34, 4, 227-235.

Clark, R.B., 2001. Marine Pollution. Oxford University Press, Oxford.

Cros, L. and García-Rey, J., 1980. Contenido en mercurio de los sedimentos marinos cercanos a la desembocadura del río Besós y de un colector de aguas residuales de Barcelona. Invest. Pesq. 44, 331-336.

Eggleton, J., Thomas, K.V., 2004. A review of factors affecting the release and bioavailability of contaminants during sediment disturbance events. Environ. Int., 30, 973– 980.

Frignani, M., Belluci, L.G., Langone, L., Muntau, H., 1997. Metal fluxes to the sediments of the northern Venice Lagoon. Mar. Chem. 58, 275–292.

Garcia-Orellana, J., Cañas, L.,Masqué, P., Obrador, B., Olid, C., Pretus, J., 2011. Chronological reconstruction of heavy metal pollution in the Port of Maó (Minorca, Spain). Mar. Pollut. Bull. 62, 1632–1640.

George, D.A., Hill, P.S., Milligan, T.G., 2007. Flocculation, heavy metals (Cu, Pb, Zn) and the sand–mud transition on the Adriatic continental shelf, Italy. Cont. Shelf Res. 27, 475–488.

Giró, S., Maldonado, A., 1985. Análisis granulométrico por métodos automáticos: tubo de sedimentación y Sedigraph. Acta Geol. Hispànica 20, 95–102.

Gómez J., Espino, M., Puigdefabregas, J., Jerez, F., 2005. Xarxa d'Instrumentació Oceanogràfica i Meteorologica de la Generalitat de Catalunya (XIOM). Boies d'onatge, dades obtingudes l'any 2004. Informe Técnico.

Grifoll, M., Gracia, V., Fernández, J., Espino, M., 2013. Suspended sediment observations in the Barcelona inner-shelf during storms. J. Coast. Res. Spec. 65, 1533–1538.

Grifoll, M., Gracia, V., Aretxabaleta, A.L., Guillén, J., Espino, M., Warner, J.C., 2014. Formation of fine sediment deposit from a flash flood river in the Mediterranean Sea. J. Geophys. Res.: Oceans 119, 5837–5853.

Guillén, J., Palanques, A., Durrieu de Madron, X., Nyffeler, F., 2000. Field calibration of optical sensors for measuring suspended sediment concentration in the western Mediterranean. Sci. Mar. 64 (4), 427–435.

Guillén, J., Bourrin, F., Palanques, A., Durrieu de Madron, X., Puig, P., Buscail, R., 2006. Sediment dynamics during wet and dry storm events on the Têt inner-shelf (SW Gulf of Lions). Mar. Geol. 234 (1–4), 129–142.

Harris, C.K., Wiberg, P.L., 1997. Approaches to quantifying long-term continental shelf sediment transport with an example from the Northern California STRESS mid-shelf site. Cont. Shelf Res. 17 (11), 1387–1418.

Harris, C.K., Wiberg, P.L., 2002. Across-shelf sediment transport: interactions between suspended sediment and bed sediment. J. Geophys. Res. 107 (C1).

Heussner, S., Ratti, C., Carbonne, J., 1990. The PPS 3 time series sediment traps and the trap sample processing techniques used during the ECOMARGE experiment. Cont. Shelf Res. 10, 943–958.

Khaled-Khodja, S., Cherif, S., Durand, G., 2018; Seasonal assessment of metal trace element contamination by PCA in Seybouse wadi (Algeria). Water Sci. Tech.-W. Sup., 18.6, 1897-1905.

Li, Y., Lin, Y., Wang, L., 2018. Distribution of heavy metals in seafloor sediments on the East China Sea inner shelf: Seasonal variations and typhoon impact. Mar. Pollut. Bull. 129, 534-544.

Liquete, C., Canals, M., Lastres, G., Amblas, D., Urgelés, R., De Mol, B., De Batis, M., Hughes-Clarke, J.E., 2007. Long-term development and current status of the Barcelona continental shelf: a source-to-sink approach. Cont. Shelf Res. 27, 1779–1800.

Liquete, C., Canals, M., Ludwig, W., Arnau, P., 2009. Sediment discharge of the rivers of Catalonia, NE Spain, and the influence of human impacts. J. Hydrol. 366, 76–88.

Long, E.R., Macdonald, D.D., Smith, S.L., Calder, F.D., 1995. Incidence of adverse biological effects within ranges of chemical concentrations in marine and estuarine sediments. Environ. Manag. 19, 81–97.

Lopes-Rocha, M., Langone, L., Miserocchi, S., Giordano, P., Guerra, R., 2017. Spatial patterns and temporal trends of trace metal mass budgets in the western Adriatic sediments (Mediterranean Sea). Sci. Total Environ. 599-600, 1022-1033.

López, L., Guillén, J., Palanques, A., Grifoll, M., 2017. Seasonal sediment dynamics on the Barcelona inner shelf (NW Mediterranean): A small Mediterranean river- and wave-dominated system, Cont. Shelf Res., 145, 80-94.

Maanan, M., 2008. Heavy metal concentrations in marine molluscs from the Moroccan coastal region. Environ. Pollut. 153 (1), 176–183.

Masson, M., Angot, H., Le Bescond, C., Launay, M., Dabrin, A., Miège, C., Le Coz, J., Coquery, M., 2018. Sampling of suspended particulate matter using particle traps in the Rhône River: relevance and representativeness for the monitoring of contaminants. Sci.Total Environ. 637–638, 538–549.

Modamio, X., 1986. Heavy Metal distribution on the Coast of California. Mar. Pollut. Bull. 17, 383-385.

Najamuddin, Prartono, T., Sanusi, H.S., Nurjaya, I.W., 2016. Seasonal distribution and geochemical fractionation of heavy metals from surface sediment in a tropical estuary of Jeneberang River, Indonesia. Mar. Pollut. Bull. 111, 456-462.

Nittrouer, C.A., Wright, L.D., 1994. Transport of particles across continental shelves. Rev. Geophys., 32, 85-113.

Oursel, B., Garnier, C., Pairaud, I., Omanovi, D., Durrieu, G., Syakti, A. D., Le Poupon, C., Thouvenin, B., Lucas, Y., 2014. Behaviour and fate of urban particles in coastal waters: Settling rate, size distribution and metals contamination characterization Estuar. Coast. Shelf Sci. 138, 14-26.

Palanques, A., Plana, F., Maldonado, A., 1990. Recent influence of man on Ebro margin sedimentation system (Northwestern Mediterranean sea). Mar. Geol. 95 (247-63).

Palanques, A., 1994. Distribution and heavy metal pollution of the suspended particulate matter on the continental shelf (North-Western Mediterranean). Environ. Pollut. 85, 205–215.

Palanques, A., Diaz, J.I., 1994. Anthropogenic heavy metal pollution in the sediment of the Barcelona continental shelf (Northwestern Mediterranean). Mar. Environ. Res. 38, 17–31.

Palanques, A., Sanchez-Cabeza, J.A., Masqué, P., Leon, L., 1998. Historical record of heavy metals in a highly contaminated Mediterranean deposit: the Besòs Prodelta. Mar. Chem. 61, 209–217.

Palanques, A., Masqué, P., Puig, P., Sanchez-Cabeza, J.A., Frignani, M., Alvisi, F., 2008. Anthropogenic trace metals in the sedimentary record of the Llobregat continental shelf and adjacent Foix Submarine Canyon (northwestern Mediterranean). Mar. Geol. 248 (3–4), 213–227

Palanques, A., Caixach, J., Belzunces, M., Bartolomé, A., 2016. Evolution of Chemical Pollution in Catalan Coastal Sediments. In: Munné, A., Ginebreda, A., Prat, N. (Eds.), Experiences from Ground, Coastal and Transitional Water Quality Monitoring. The EU Water Framework Directive Implementation in the Catalan River Basin District 2. Springer, Switzerland, pp. 271–300.

Palanques, A., López, L., Guillén, J., Puig, P., Masqué, P., 2017. Decline of trace metal pollution in the bottom sediments of the Barcelona City continental shelf (NW Mediterranean). Sci. Total Environ. 579, 755-767.

Palinkas, C., Nittrouer, C., 2007. Modern sediment accumulation on the Po shelf, Adriatic Sea. Cont. Shelf Res. 27, 489–505.

Poulton, S.W., Raiswell, R., 2000. Solid phase associations, oceanic fluxes and the anthropogenic perturbation of transition metals in world river particulates. Mar. Chem. 72, 17-31.

Puig, P., Palanques, A., Sánchez-Cabeza, J.A., Masqué, P., 1999. Heavy metals in particulate matter and sediments in the southern Barcelona sedimentation system (Northwestern Mediterranean). Mar. Chem. 63, 311–329.

Querol, X., Alastuey, A., Lopez Soler, A., Mantilla, E., Plana, F., 1996. Mineralogy of atmospheric particulates around a large coal-fired power station. Atmos. Environ. 30 (21), 3557–3572.

Radakovitch, O., Roussiez, V., Ollivier, P., Ludwig, W., Grenz, C., Probst, J.-L., 2008. Input of particulate heavy metals from rivers and associated sedimentary deposits on the Gulf of Lion continental shelf. Estuar. Coast. Shelf S. 77, 285-295.

Rodellas, V., Garcia-Orellana, J., Masqué, P., Feldman, M., Weinstein, Y., 2015. Submarine groundwater discharge as a major source of nutrients to the Mediterranean Sea. PNAS 112, 13, 3926-3930.

Roussiez, V., Ludwig, W., Monaco, A., Probst, J. L, Bouloubassi, I., Buscail, R., Saragoni, G., 2006. Sources and sinks of sediment-bound contaminants in the Gulf of Lions (NW Mediterranean Sea): a multi-tracer approach. Cont. Shelf Res. 26, 1843-1857.

Sancho-García, A., Guillén, J., Ojeda, E., 2013. Storm-induced readjustment of an embayed beach after modification by protection works. Geo-Mar. Lett. 33, 159–172.

Schwarzenbach, R. P., Escher, B. I., Fenner, K., Hofstetter, T. B., Johnson, C. A., von Gunten, U., Wehrli, B., 2006. The Challenge of Micropollutants in Aquatic Systems. Science, 313. 1072-1077.

Spanish Port Authority, 2016. Puertos del Estado. Oceanografía y Meteorología. Banco de datos. Punto WANA 2066051. ⟨http://www.puertos.es/es-es/oceanografia/Portus/ Paginas/Portus.aspx⟩. (Last accessed: March 2016).

Spencer, K.L., Cundy, A.B., Croudace, I.W., 2003. Heavy metal distribution and early-diagenesis in salt marsh sediments from the Medway estuary, Kent, UK. Estuar. Coast. Shelf Sci. 57 (1–2), 43–54.

Stevens, A.W., Wheatcroft, R.A., Wiberg, P.L., 2007. Seabed properties and sediment erodibility along the western Adriatic margin, Italy. Cont. Shelf Res. 27, 400-416.

Tan, K.S., Denil, D.J., Ransangan, J., 2016. Temporal and spatial variability of heavy metals in Marudu Bay, Malaysia. Oceanol Hydrobiol St., 45, 353-367.

Tansel, B., Rafiuddin, S., 2016. Heavy metal content in relation to particle size and organic content of surficial sediments in Miami River and transport potential. Int. J. Sediment Res. 31, 324–329.

US EPA, 2007. Method 7473. Mercury in Solids and Solutions by Thermal Decomposition, Amalgamation, and Atomic Absortion Spectrophotometry (http://www.epa.gov/osw/hazard/testmethods/sw846/pdfs/7473.pdf).

Viers, J., Dupré, B., Gaillardet, J., 2009. Chemical composition of suspended sediments in World Rivers: New insights from a new database. Sci. Total Environ., 407, 2, 853 – 868.

Wang, H., Wang, J., Liu, R., Yu, W., Shen, Z., 2015. Spatial variation, environmental risk and biological hazard assessment of heavy metals in surface sediments of the YangtzeRiver estuary. Mar. Pollut. Bull. 93, 250–258.

Warren, C., Duzgoren-Aydin, N.S., Weston, J., Willett, K.L., 2012. Trace element concentrations in surface estuarine and marine sediments along the Mississippi Gulf Coast following Hurricane Katrina. Environ. Monit. Assess. 184:1107–1119.

Wheatcroft, R.A., Borgeld, J.C., 2000. Oceanic flood deposits on the northern California shelf: large-scale distribution and small-scale physical properties. Cont. Shelf Res., 20, 2163–2190.

Wiberg, P., Smith, J.D., 1983. A comparison of field data and theoretical models for wave–current interactions at the bed on the continental shelf. Cont. Shelf Res. 2, 147–162.

Wiberg, P.L., Drake, D.E., Cacchione, D.A., 1994. Sediment resuspension and bed armoring during high bottom stress events on the northern California continental shelf: measurements and predictions. Cont. Shelf Res. 14, 1191–1219. Res. 2, 147–162.

Figure Captions

Figure 1. Map showing the study area and the location of the stations where sediment cores were taken and instrumented tripods were installed. WTP, Barcelona Besòs waste water treatment plant. 20 m-site (Be20). 30 m-site (Be30). Grey dash line: limit of the muddy prodelta

Figure 2. Time series of a) river discharge, b) wave direction, c) significant wave height, d) current speed, e) total bottom shear stress, f) suspended sediment concentration and d) trapped total mass flux recorded in the study area (location in Fig. 1). Black lines, records from the 20 m depth site. Red line, records from the 30 m depth site.

Figure 3. Time series of a) mud (silt+clay) content, b) total organic carbon (TOC) and, c) aluminium (Al) content in the trapped particulate matter at the study sites (location in Fig. 1). Black arrows represent the 12 wave storm events

described in Table 1, which increased SSC significantly; grey dash lines, the time when sediment cores were taken. Black lines with circles, records from the 20 m depth site. Red lines with triangles, records from the 30 m depth site

Figure 4. Time series of TM (Cr, Pb, Cd, Hg, Cu and Zn) content in the trapped particulate matter at the study sites (location in Fig. 1). Black lines with cercles, records from the 20 m depth site. Red lines with triangles, records from the 30 m depth site. Data in mg kg^{-1}. Black arrows represent the 12 wave storm events described in Table 1, which increased SSC significantly; grey dash lines, the time when sediment cores were taken.

Figure 5. Time series of TM_n (Cr_n, Pb_n, Cd_n, Hg_n, Cu_n and Zn_n) content in the trapped particulate matter at the study sites (location in Fig. 1). Black lines with circles, records from the 20 m depth site. Red lines with triangles, records from the 30 m depth site. Data in mg kg^{-1}. Black arrows represent the 12 wave storm events described in Table 1, which increased SSC significantly; grey dashed lines, the time when sediment cores were taken.

Figure 6. Time series of trapped Cr, Pb, Cd, Hg, Cu and Zn fluxes at the study sites (location in Fig. 1). Black lines, records from the 20 m depth site. Red line, record from the 30 m depth site. Data in mg m^{-2} d^{-1}. Black arrows represent the 12 wave storm events described in Table 1, which increased SSC significantly; grey dash lines, the time when sediment cores were taken.

Figure 7. Vertical distributions of mud (silt + clay), total organic carbon (TOC), and Al content in the sediment cores taken at the study sites.

Figure 8. Vertical distribution of the TM contents in the sediment cores taken at the study sites. Data in mg kg^{-1}. A, inflexion points where TM reached maximum values (See that they are at different depths in each sediment core).

Figure 9. Vertical distribution of the TM_n contents in the sediment cores taken at the study sites. Data in mg kg^{-1}. A, inflexion points where TM reached maximum values (See that they are at different depths in each sediment core).

Figure 10. River discharge, Total bottom shear stress, Hg_n of trapped particulate matter and Hg_n in the studied sediment cores. The sediment cores are represented taking as a common reference depth the inflexion point of the maximum Hg_n value (black dashed line). The pink dashed lines follow the top of the cores to show the erosive and depositional trend of each one in relation to the September core. Black dots, 20 m depth site; red dots 30 m depth site. Hg concentrations in mg kg^{-1}.

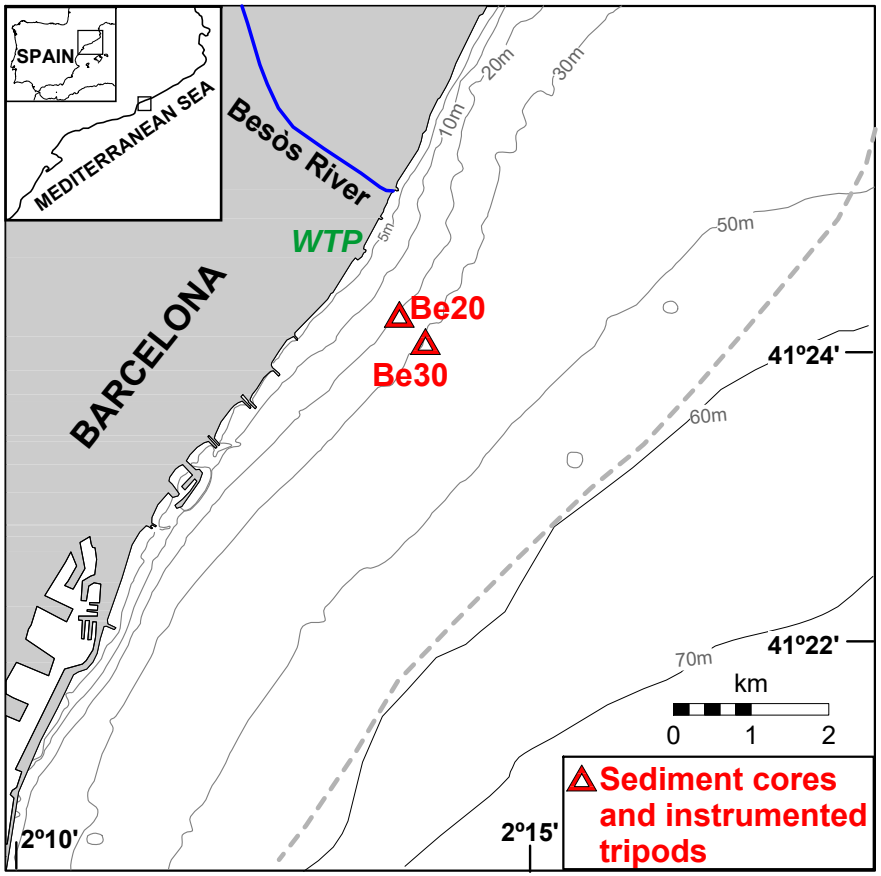
SPAIN
MEDITERRANEAN SEA
Besòs River
WTP
BARCELONA
Be20
Be30
5m
10m
20m
30m
50m
60m
70m
41°24'
41°22'
km
0
1
2
Sediment cores and instrumented tripods
2°10'
2°15'

Fig. 1

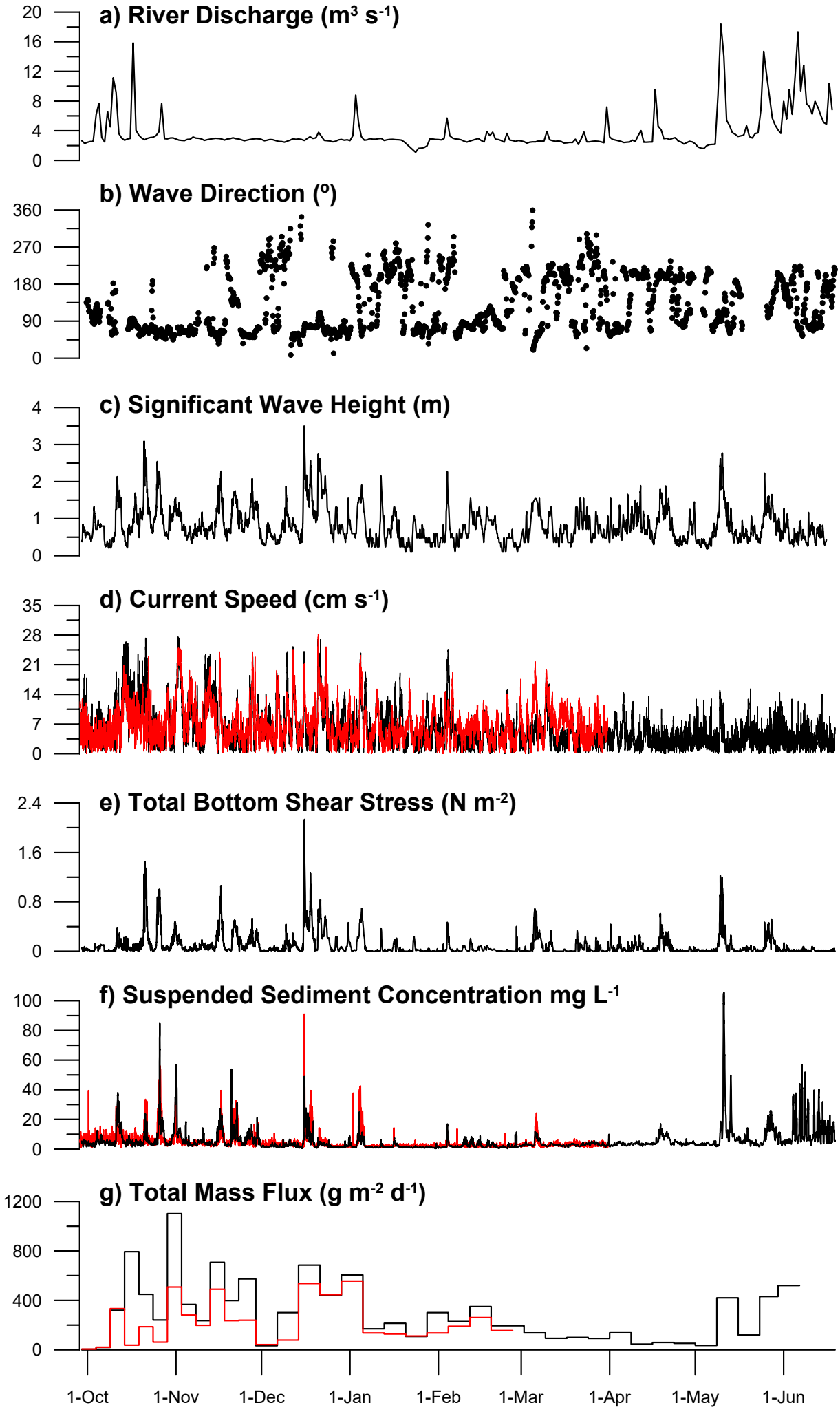
a) River Discharge (m³ s⁻¹)
20
16
12
8
4
0
b) Wave Direction (º)
360
270
180
90
0
c) Significant Wave Height (m)
4
3
2
1
0
d) Current Speed (cm s⁻¹)
35
28
21
14
7
0
e) Total Bottom Shear Stress (N m⁻²)
2.4
1.6
0.8
0
f) Suspended Sediment Concentration mg L⁻¹
100
80
60
40
20
0
g) Total Mass Flux (g m⁻² d⁻¹)
1200
800
400
0
1-Oct
1-Nov
1-Dec
1-Jan
1-Feb
1-Mar
1-Apr
1-May
1-Jun

Fig. 2

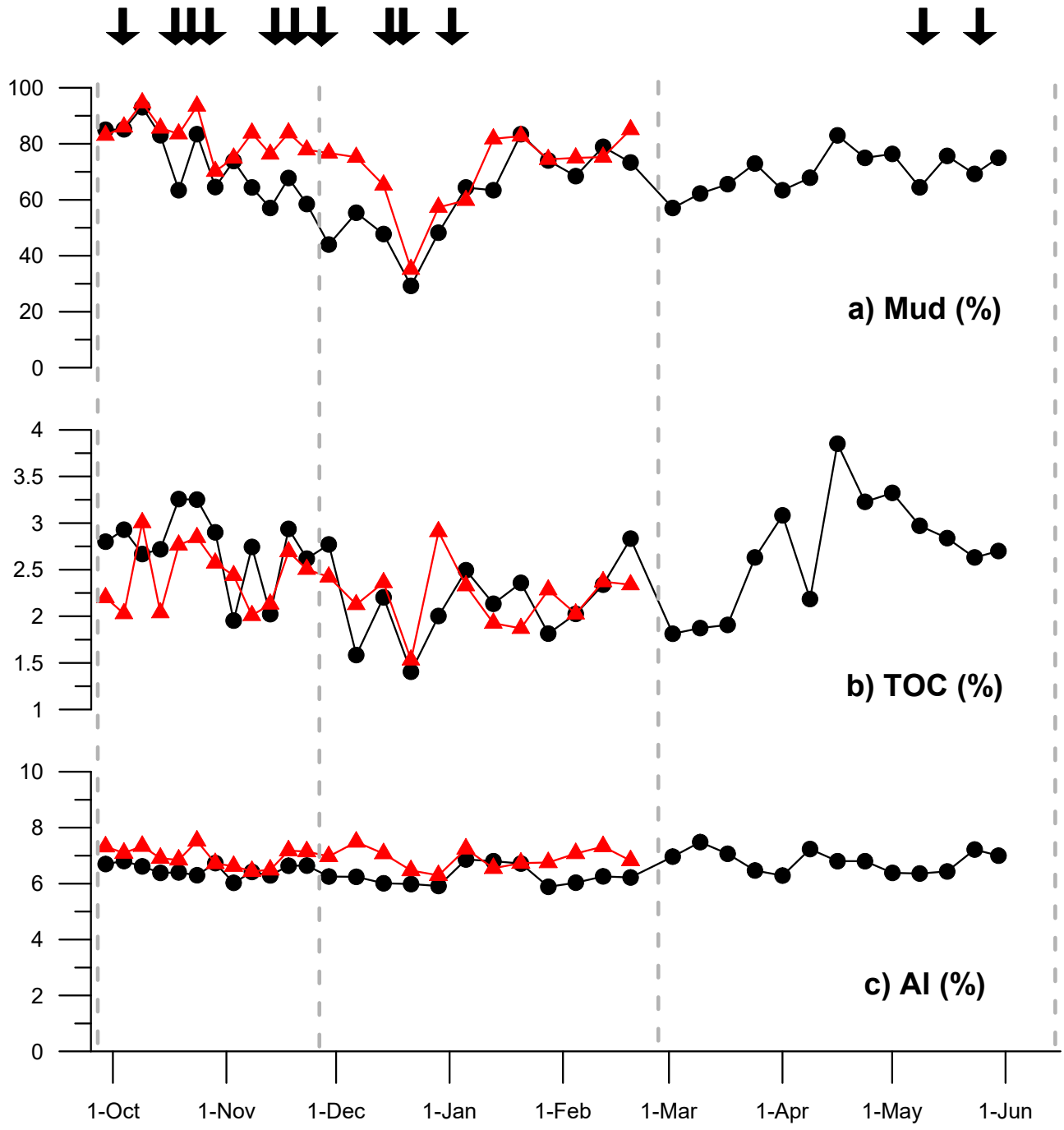
100
80
60
40
20
0
a) Mud (%)
4
3.5
3
2.5
2
1.5
1
b) TOC (%)
10
8
6
4
2
0
c) Al (%)
1-Oct
1-Nov
1-Dec
1-Jan
1-Feb
1-Mar
1-Apr
1-May
1-Jun

Fig. 3

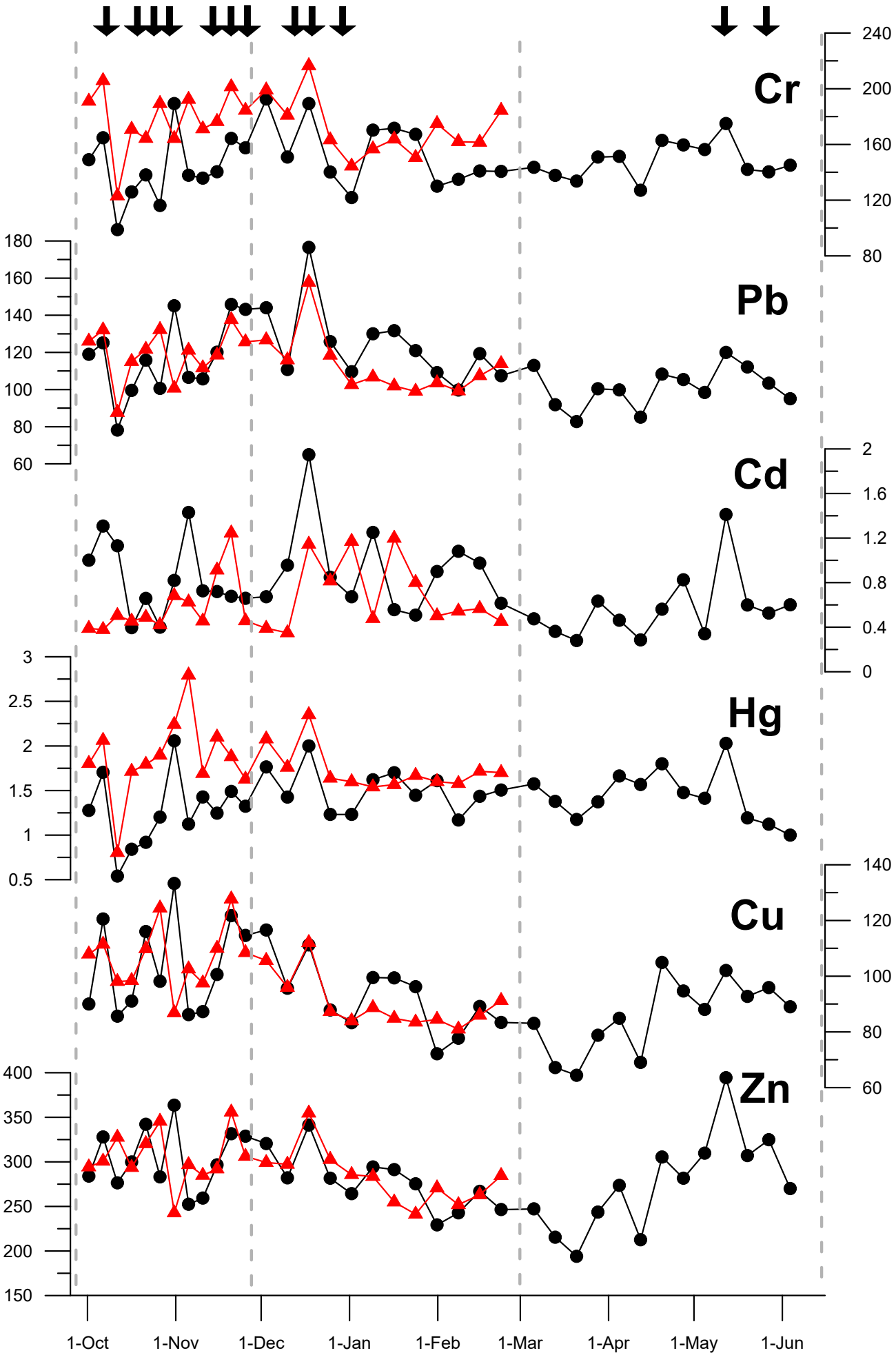
Cr
Pb
Cd
Hg
Cu
Zn
240
200
160
120
80
180
160
140
120
100
80
60
2
1.6
1.2
0.8
0.4
0
3
2.5
2
1.5
1
0.5
140
120
100
80
60
400
350
300
250
200
150
1-Oct
1-Nov
1-Dec
1-Jan
1-Feb
1-Mar
1-Apr
1-May
1-Jun

Fig. 4

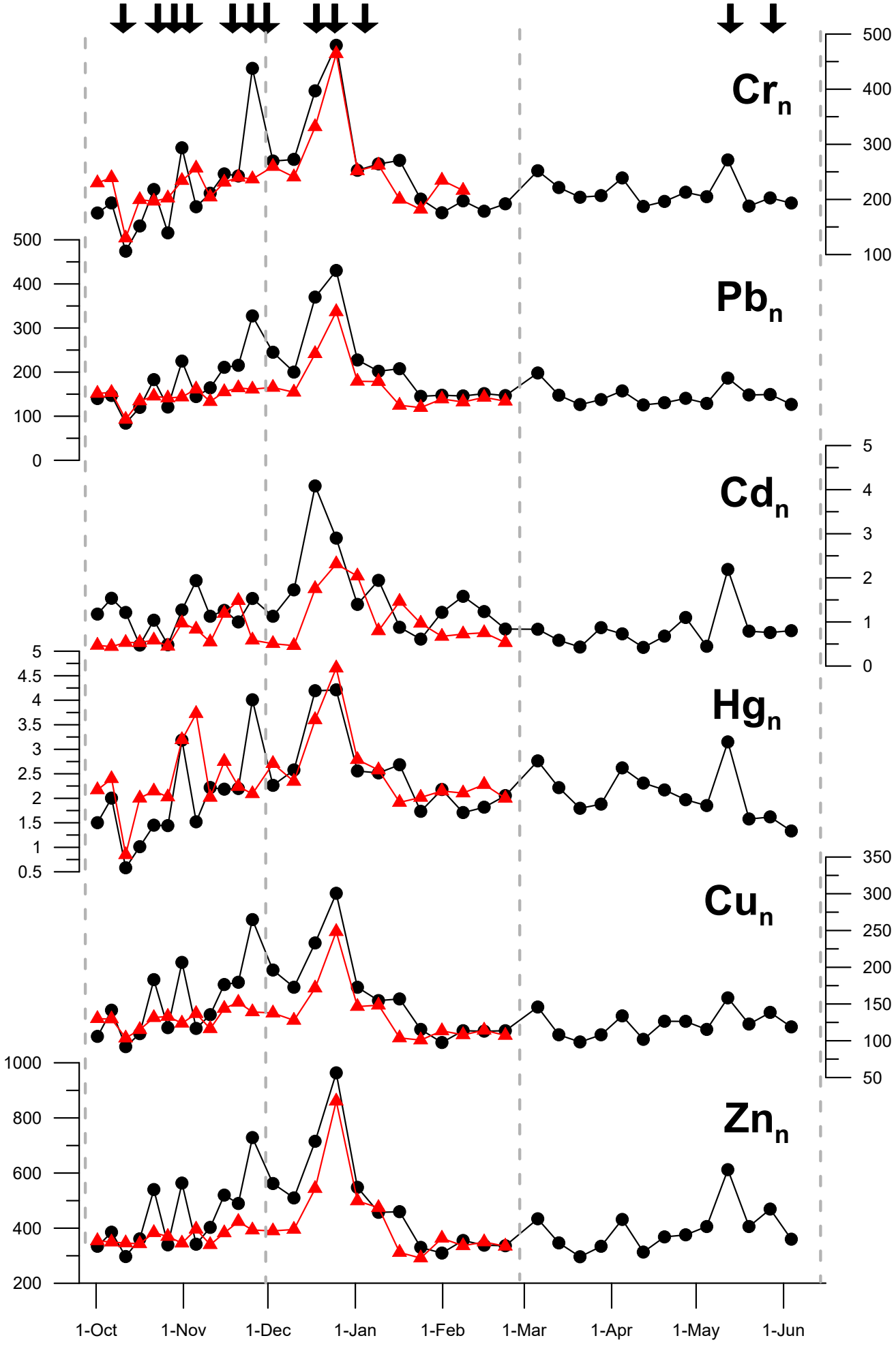
Cr_n
Pb_n
Cd_n
Hg_n
Cu_n
Zn_n
1-Oct
1-Nov
1-Dec
1-Jan
1-Feb
1-Mar
1-Apr
1-May
1-Jun

Fig. 5

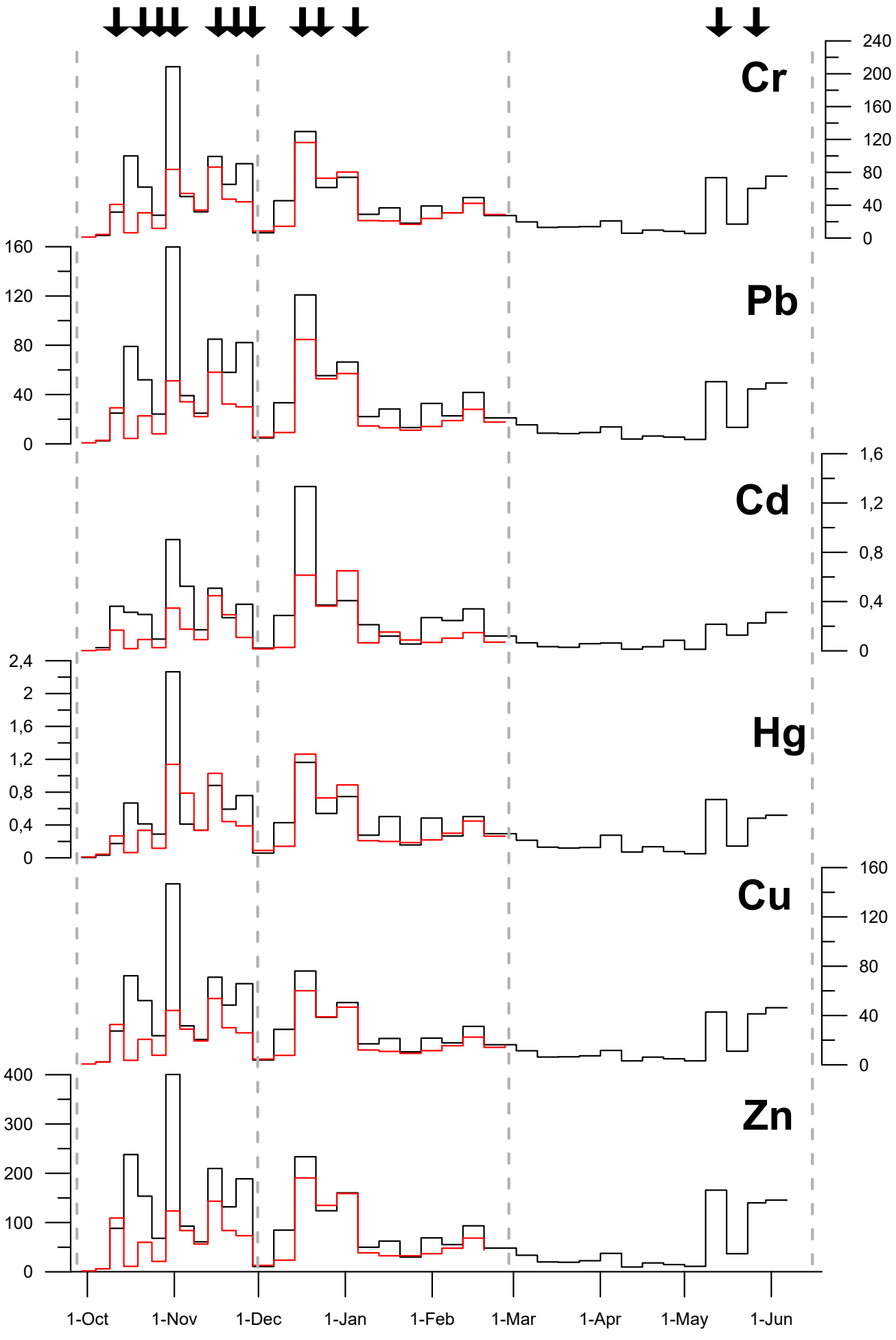

Palanques et al. Fig. 6

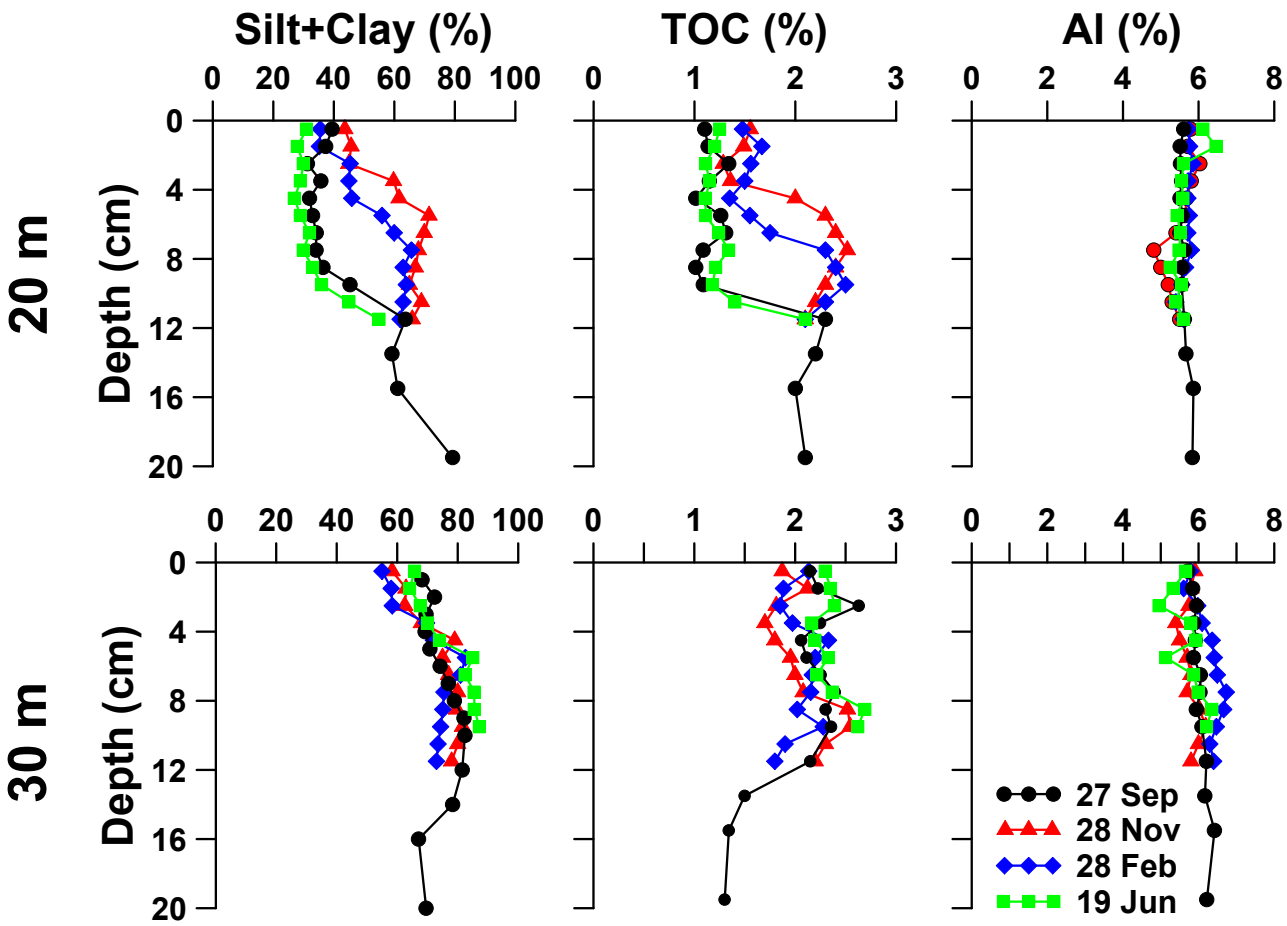
Silt+Clay (%)
TOC (%)
Al (%)
20 m
30 m
Depth (cm)
0 20 40 60 80 100
0 1 2 3
0 2 4 6 8
0 4 8 12 16 20
27 Sep
28 Nov
28 Feb
19 Jun

Fig. 7

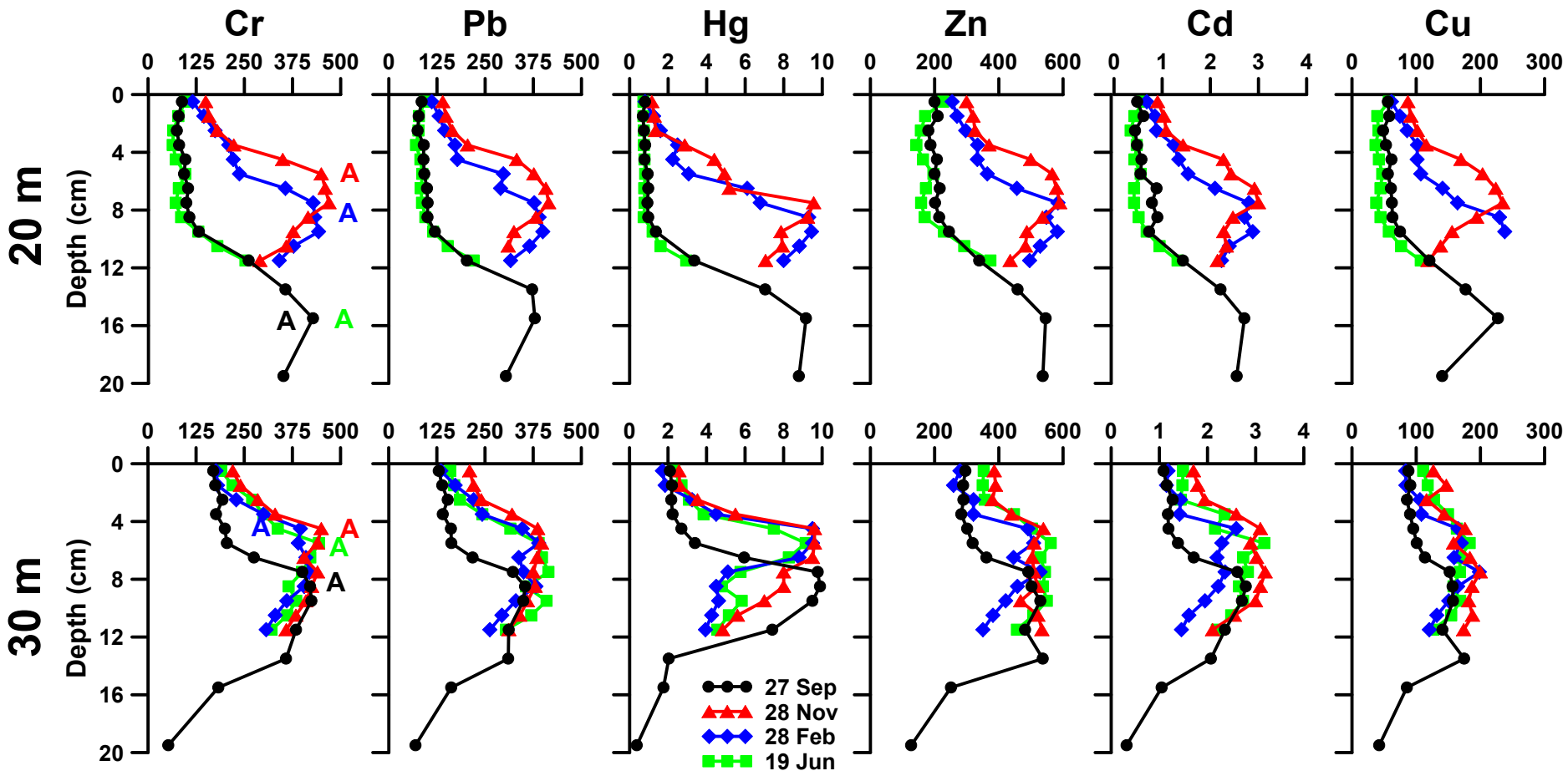
Cr
Pb
Hg
Zn
Cd
Cu
20 m
30 m
Depth (cm)
0 125 250 375 500
0 2 4 6 8 10
0 200 400 600
0 1 2 3 4
0 100 200 300
0 4 8 12 16 20
A
27 Sep
28 Nov
28 Feb
19 Jun

Fig. 8

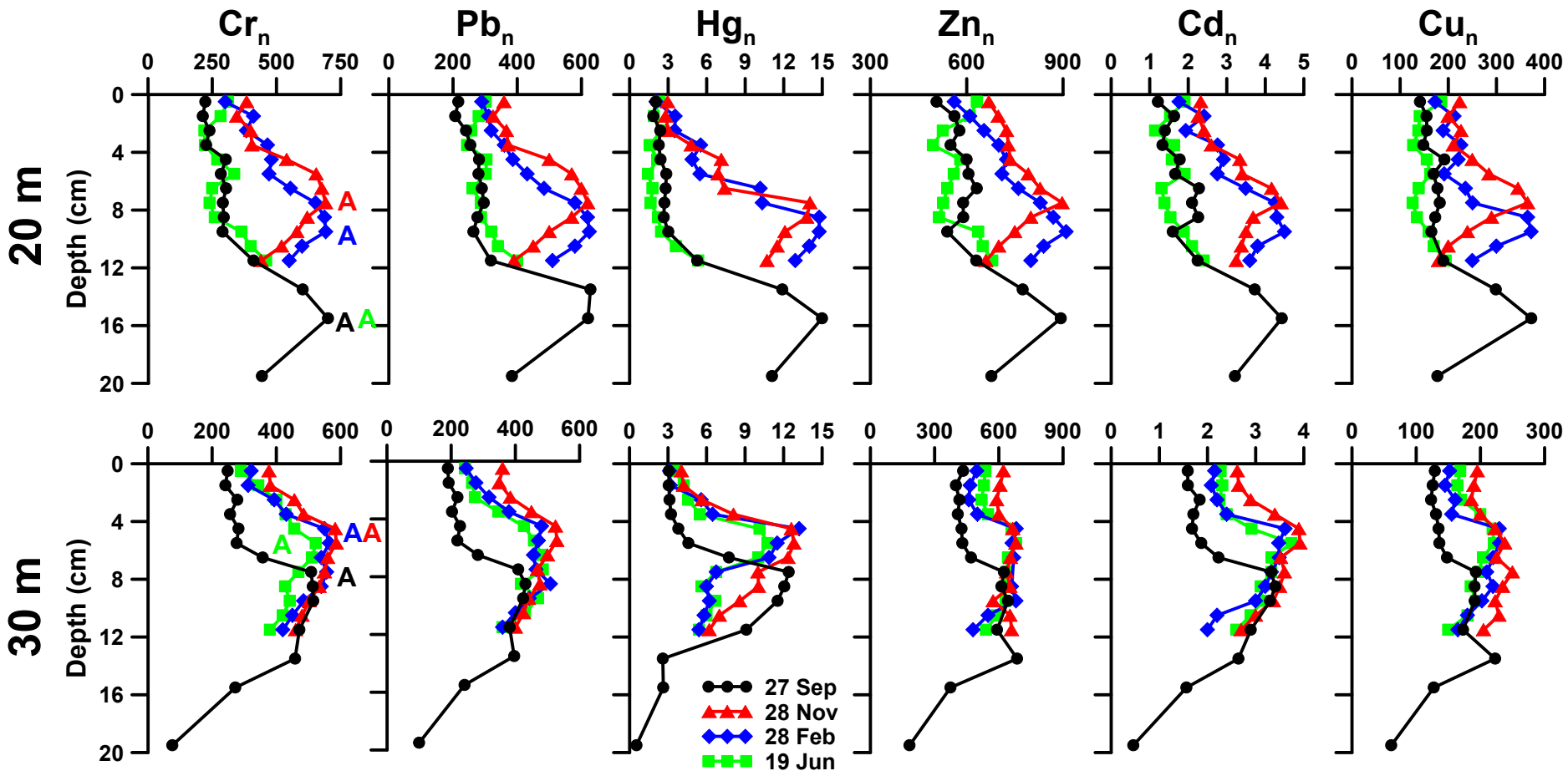
Cr$_n$
Pb$_n$
Hg$_n$
Zn$_n$
Cd$_n$
Cu$_n$
20 m
30 m
Depth (cm)
A
A
A
A
A
A
27 Sep
28 Nov
28 Feb
19 Jun

Fig. 9

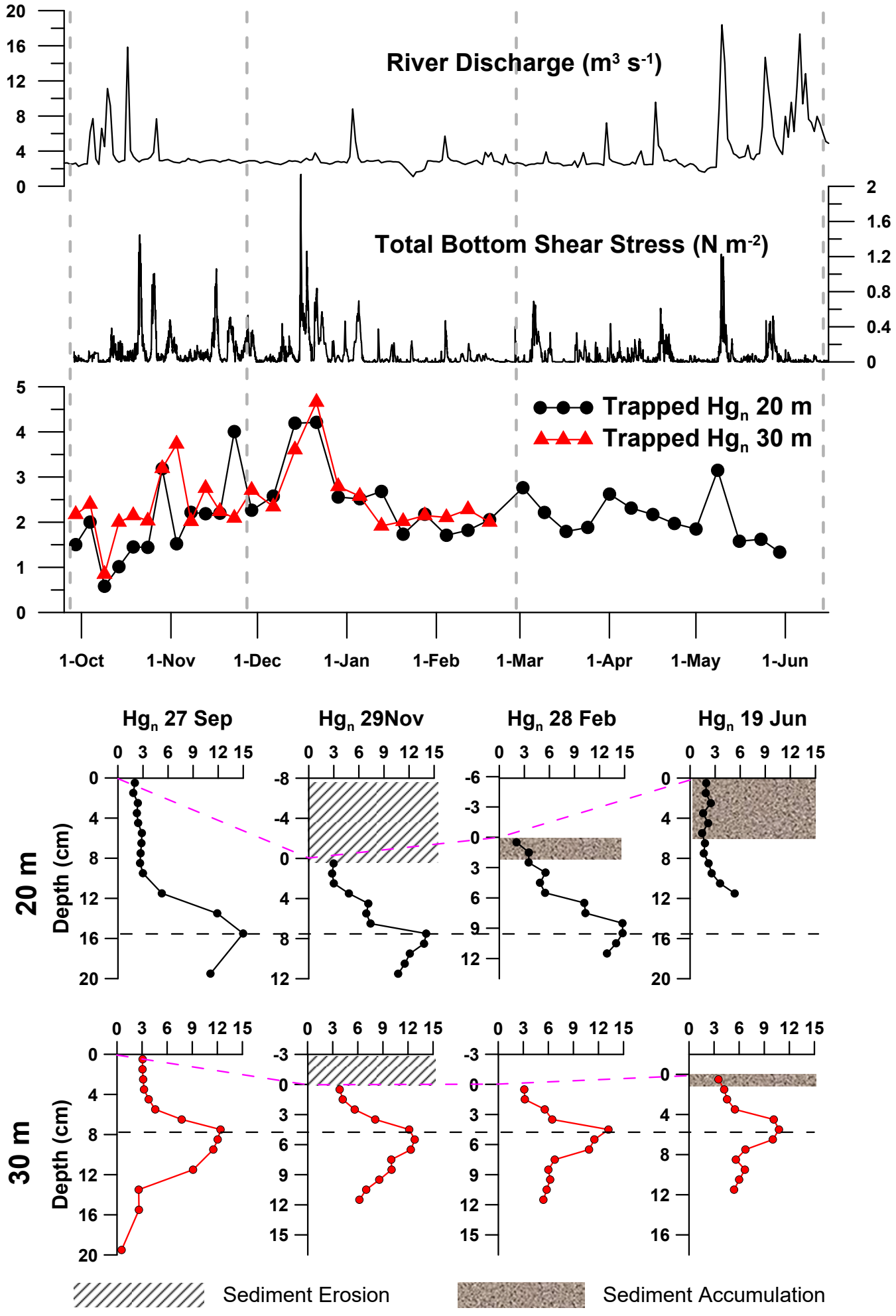
River Discharge (m³ s⁻¹)
Total Bottom Shear Stress (N m⁻²)
Trapped Hgn 20 m
Trapped Hgn 30 m
1-Oct
1-Nov
1-Dec
1-Jan
1-Feb
1-Mar
1-Apr
1-May
1-Jun
Hgn 27 Sep
Hgn 29Nov
Hgn 28 Feb
Hgn 19 Jun
20 m
30 m
Depth (cm)
Sediment Erosion
Sediment Accumulation

Fig. 10

Table 1

Characteristics of storm events at 20m depth during the deployment period. Wave ht., significant wave height. Wave Tp., wave period. S. str., total shear stress. SSC, suspended sediment concentration. Cu. sp., current speed. Rv. ds., river discharge. Wave dir., wave direction. Dur., duration.

Date	*Wave ht. (m)*	*Wave Tp. (s)*	*S. str. ($N\ m^{-2}$)*	*SSC ($mg\ L^{-1}$)*	*Cu. sp. ($cm\ s^{-1}$)*	*Rv. ds. (m^3)*	*Wave dir. (^{o})*	*Dur. (h)*
11-Oct	2.3	7.1	0.38	39.3	18	9.1	82	29
20-Oct	3.09	10.5	1.44	22.3	24	2.8	77	35
25-Oct	2.54	12.5	1.00	82.3	8	7.7	76	36
31-Oct	1.57	11.1	0.48	58	28	2.9	132	72
16-Nov	2.28	11.8	1.05	27	21	3	92	29
21-Nov	1.75	9.1	0.50	57.7	15	3	87	56
27-Nov	2.08	9.1	0.53	21.6	23	3	83	90
15-Dec	3.38	11.1	2.09	48.9	0.24	3	87	93
20-Dec	2.74	8	0.68	3.5	14	3	84	74
4-Jan	1.90	10	0.69	24.1	24	6.1	55	61
09-May	2.77	10	1.22	103.7	15	18.4	131	48
25-May	2.23	9.1	0.47	38	12	11.8	111	86

Table 2

Pearson correlation matrix of the TM_n in the trapped particulate matter and the maximum and mean shear stress (MX SS and MN SS respectively) during every sampling period of the sediment traps **correlated variables.

	Cr	Pb	Ni	Zn	Hg	Cd	Cu	MX SS	MN SS
Cr	1								
Pb	,958**	1							
Ni	,848**	,863**	1						
Zn	,914**	,932**	,947**	1					
Hg	,845**	,751**	,589**	,671**	1				
Cd	,647**	,703**	,567**	,590**	,426*	1			
Cu	,903**	,945**	,907**	,965**	,676**	,606**	1		
MX SS	,497**	,559**	,549**	,601**	,528**	,465**	,567**	1	
MN SS	,449**	,543**	,556**	,603**	,506**	,438**	,616**	,939**	1

Table 3

TM and TM_n contents of the surface sediment samples taken in the sediment cores at 20 m and 30 m depth. Concentrations in mg kg^{-1}.

20 m depth	Cr	Pb	Cd	Cu	Zn	Hg
Sep	88.08	85.58	0.48	55.89	199.85	0.80
Nov	150.45	140.31	0.90	87.26	300.83	1.16
Feb	116.02	111.68	0.68	66.62	255.15	0.79
Jun	96.74	93.68	0.59	57.44	226.84	0.72
	Cr_n	Pb_n	Cd_n	Cu_n	Zn_n	Hg_n
Sep	222.93	216.59	1.21	141.45	505.81	2.03
Nov	384.61	358.97	2.32	223.75	669.23	2.96
Feb	300.73	289.48	1.76	172.68	561.36	2.06
Jun	312.09	302.21	1.90	185.30	631.75	2.32

30 m depth	Cr	Pb	Cd	Cu	Zn	Hg
Sep	169.38	129.6	1.09	87.99	295.83	2.09
Nov	220.02	210.05	1.71	126.73	386.08	2.57
Feb	176.82	135.72	1.18	83.76	278.78	1.71
Jun	190	159.87	1.49	110.92	353.16	2.32
	Cr_n	Pb_n	Cd_n	Cu_n	Zn_n	Hg_n
Sep	248.21	189.91	1.59	128.94	433.52	3.07
Nov	377.23	360.08	2.62	195.24	621.87	4.04
Feb	321.48	246.77	2.15	152.29	496.88	3.11
Jun	319.06	243.22	2.27	168.76	537.29	3.53

Table S1

Minimum, maximum and mean background trace metal levels normalized to aluminium content in the sediment cores taken at 20 and 30 m depth. Concentrations in mg kg^{-1}.

Depth	Value	Hg	Zn	Cr	Pb	Cd	Cu
20 m	Min-max	0.04-0.07	78.7-82.6	53.0-56.3	23.0-39.4	0.14-0.15	21.1-22.4
	Mean	*0.05*	*79.9*	*53.9*	*29.4*	*0.15*	*21,5*
30 m	Min-max	0.07-0.09	81.0-89.3	54.9-62.1	37.1-48.1	0.15-0.16	21.9-24.8
	Mean	*0.08*	*85.0*	*58.3*	*42.9*	*0.16*	*23.3*

Table S2

Pearson correlation matrix of the TM, Al, TOC and mud (silt + clay) of the sediment cores taken at 20 and 30 m depth **correlated variables.

	Al	Cr	Pb	Cd	Cu	Zn	Hg	TOC	Mud
Al	1								
Cr	.170	1							
Pb	.178	.980**	1						
Cd	.124	.974**	.969**	1					
Cu	.098	.963**	.953**	.952**	1				
Zn	.123	.973**	.967**	.971**	.970**	1			
Hg	.086	.914**	.899**	.924**	.860**	.884**	1		
TOC	.160	.790**	.746**	.785**	.772**	.780**	.708**	1	
Mud	.430**	.748**	.708**	.732**	.678**	.695**	.680**	.759**	1

Table S3

Minimum, maximum and mean enrichment factors (EF) of the trace metals in the sediment cores taken at 20 and 30 m depth.

Depth	Value	Hg (EF)	Zn (EF)	Cr (EF)	Pb (EF)	Cd (EF)	Cu (EF)
20 m	Min-max	14.8-131.5	2.3-6.6	1.4-7.6	2.8-10.2	3.0-17.9	2.3-10.5
	Mean	*44.8*	*3.5*	*3.1*	*4.9*	*7.4*	*4.1*
30 m	Min-max	1.6-113.2	1.1-6.2	1.0-7.4	1.0-7.3	1.8-18.3	1.2-7.3
	Mean	*46.3*	*3.9*	*4.1*	*4.4*	*9.6*	*4.4*